Supporting Information

Eberlin et al. 10.1073/pnas.1409778111

SI Discussion

Some of the changes we observe in the lipid profiles could reflect differences between naive thymic and activated tumor-derived T cells. However, because the lipid signature we identify appears to distinguish v-myc avian myelocytomatosis viral oncogene homolog (MYC) from rat sarcoma (RAS)-induced lymphomas, we presume that many of these changes are causally specific to MYC, but this remains to be examined. We note that naive T cells rely on the cytokine interleukin (IL)-7 for a highly oxidative metabolic phenotype because of complete metabolism of glucose and glutamine (1). When a T cell becomes activated to mount an immune response, it undergoes a shift in metabolism. Activated inflammatory T cells or effector T cells highly depend on glucose consumption to support this proliferative phenotype. T-cell receptor stimulation is necessary for initial glucose transporter upregulation, causing an overall increased glycolysis in proliferating T cells. Increased glucose uptake fluxes through the glycolytic pathway to support ATP production, as well as lipid precursors. Some investigators have proposed that activation of Raptor-mTORC1 integrates T-cell receptor and CD28 costimulatory signals in antigen-stimulated T cells, leading to up-regulation of glycolysis and lipid synthesis (2). In contrast, resting T cells, including T regs, oxidizes fatty acids instead of synthesizing them. Thus, we would expect a higher relative lipid composition overall in activated T cells relative to resting T cells.

SI Materials and Methods

Animal Samples. Transgenic mice that exhibit conditional expression of the human c-MYC oncogene were generated for these experiments by crossing TetO-MYC transgenic mice with the Emu-tTA transgenic line. Transgenic Emu-tTA/TetO-MYC mice were bred and maintained with doxycycline (DOX, 100 μg/mL), and MYC expression was induced by subsequently removing the DOX from the drinking water (MYC ON), ultimately resulting in lymphoma formation. Thymus tissues were collected from mice once tumors were observed. Normal thymus tissues were also collected from control normal mice. All procedures were performed in accordance with Administrative Panel on Laboratory Animal Care protocols. Lymphoma tissues were collected from mice after MYC suppression for different lengths of time (0, 2, 4, 6, 8, 12, 16, 20, and 24 h). After 6–16 mo of oncogene activation, MYC ON, RAS ON and control animals were killed and the thymus tissue was collected. Tissue samples were stored in a −80 °C freezer until sectioned to 15-μm-thick sections using a Leica CM1950 cryostat (Leica Microsystems Inc.). The tissue sections were mounted onto a glass slide and stored in a −80 °C freezer. Before desorption electrospray ionization mass spectrometric imaging (DESI-MSI), the glass slides were dried in a dessicator for ∼10 min.

Cells. Cell lines isolated from our MYC or RAS-induced lymphoma models were subjected to doxycycline to shut down oncogene expression. Tumor cells were harvested at different time points following oncogene suppression (0, 4, 8, 16, 20, 24, 48, and 72 h). The cells were deposited onto glass slides and directly analyzed by DESI-MS. Three samples of each cell line were analyzed by DESI-MSI.

Human Lymphoma Tissues. Fifteen frozen human lymphoma specimens were obtained from Stanford University Tissue Bank under approved Institutional Review Board protocol. Samples were stored in a −80 °C freezer until sectioned. Human tissue samples were prepared and analyzed using the same approach described for animal samples.

DESI-MSI. A laboratory-built DESI-MSI source coupled to an LTQ-Orbitrap-XL mass spectrometer (Thermo Fisher Scientific) was used for tissue imaging. DESI-MSI was performed in the negative ion mode from *m/z* 90–1,200, with a spatial resolution of 200 μm, and using the Orbitrap as the mass analyzer set to 60,000 resolving power. The histologically compatible solvent system dimethylformamide:acetonitrile 1:1 (vol/vol) was used for analysis, at a flow rate of 0.8 μL/min. After DESI-MS imaging, the same tissue section was subjected to H&E staining for histopathological evaluation.

Lipid Identification. Identification of the molecular species was performed using tandem MS experiments and high mass resolution experiments. Tandem MS experiments were performed using the linear ion trap analyzer (LTQ) of the hybrid mass spectrometer. The mass spectra patterns obtained were compared with reported literature to allow for lipid identification in combination with high mass accuracy measurements from the Orbitrap imaging data. The LipidMaps database (www.lipidmaps.org/) was also used to assist in lipid identification.

Histopathology. After DESI-MSI, the imaged tissue sections were subjected to standard H&E staining protocol. Pathological evaluation was then performed by Richard Luong using light microscopy. Regions of homogenous cancer were carefully diagnosed and delineated before data extraction and statistical analysis.

Data and Statistical Analysis. Mass spectra from regions of clear diagnosis as determined by histopathologic evaluation were extracted from 2D data using Xcalibur Software (Thermo Fisher Scientific). The data were first converted from profile to centroid using custom-built software provided by Thermo Fisher Scientific. The centroid data were then converted to text files and imported in R language for significance analysis of microarrays (SAM) analysis. Before SAM, a rule was applied that only ions that appeared in at least 5 pixels of a sample would be considered, so that ions of low relative abundance inconsistently observed across different samples would be disregarded. SAM identifies statistically significant molecules by computing a T statistic (score) "dj" for each molecule "j" that measures the average change in the peak height (extracted ion abundance) for that molecule between different phenotypes. Repeated permutations of the data were used to determine if the expression of any molecule is significantly related to a phenotype.

Western Blot Analysis. Whole cell lysates were isolated from MYC-driven lymphoma mice samples (A,B,C–MYC ON) and normal mice thymus samples (TY, T01, T02) were loaded on an SDS/PAGE and immunoblotted with anti-MYC and anti–α-tubulin antibodies.

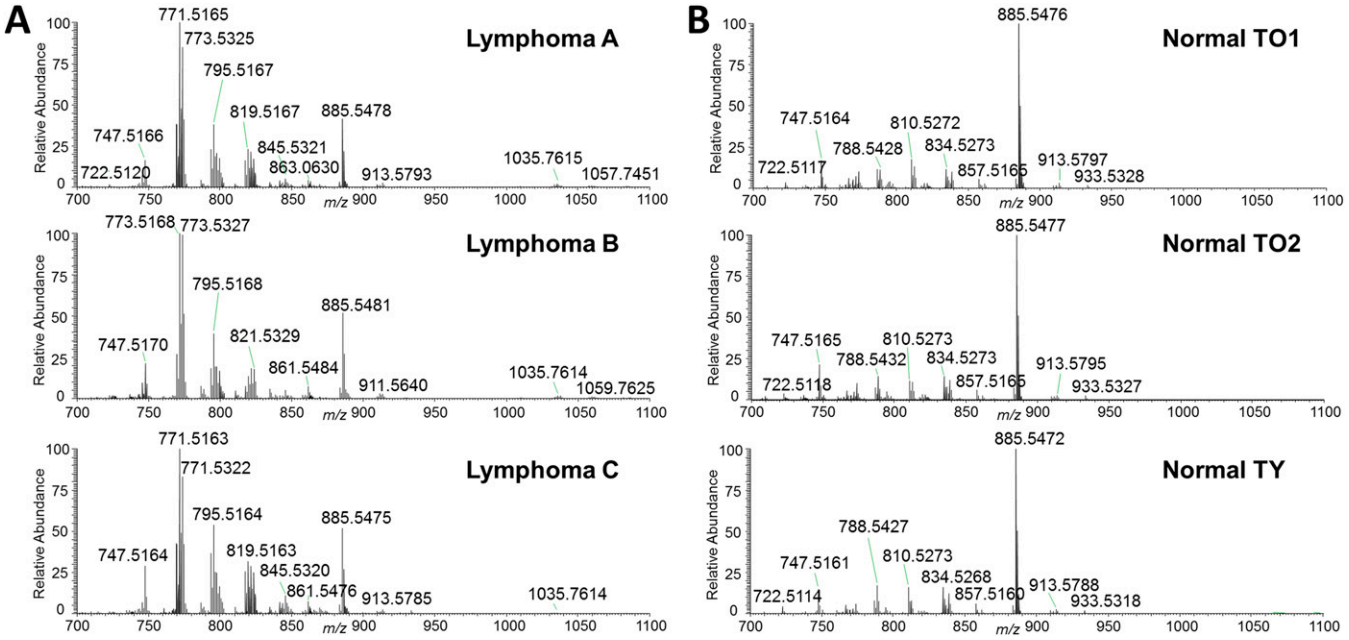

Fig. S1. DESI-MSI of MYC-induced lymphomas shows specific lipid signature. Representative negative ion mode DESI mass spectra of (*A*) MYC-induced lymphomas (samples lymphoma A, B, and C) and (*B*) Normal control thymus (samples T01, T02, and TY) tissues in the *m/z* 700–1,100 range are shown.

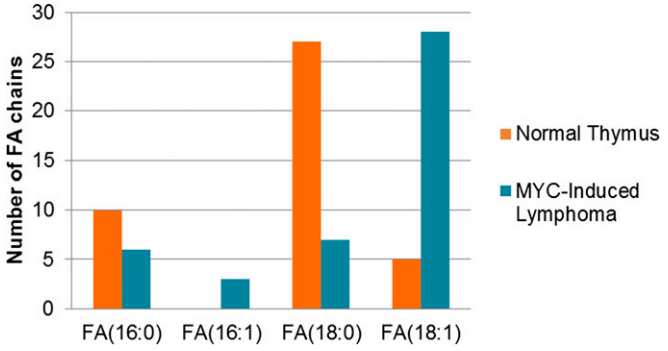

Fig. S2. Alteration in the saturation of the fatty acid (FA) chains constituents of the glycerophospholipids in lymphoma tissue in comparison with normal thymus tissue. A higher number of the monounsaturated palmitoleic acid FA(16:1) and oleic acid FA(18:1) was observed as FA chains in the glycerophospholipids found in increased abundance in lymphoma tissue compared with their saturated counterparts palmitic acid FA(16:0) and stearic acid FA(18:0), respectively.

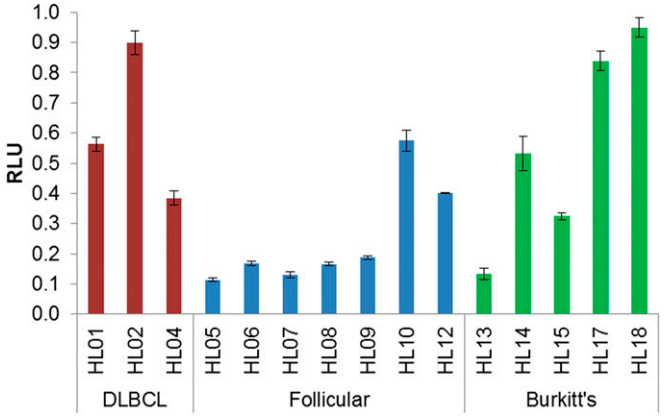

Fig. S3. Normalized nanofluidic proteomic immunoassay (NIA) data from the analysis of MYC oncoprotein expression in a set of 15 clinical specimens, including 3 diffuse large B-cell lymphoma (DLBCL), 7 follicular lymphoma, and 5 Burkitt's lymphoma. Data are represented as the normalized peak areas detected by NIA; mean of 4 replicates per sample ±SEM.

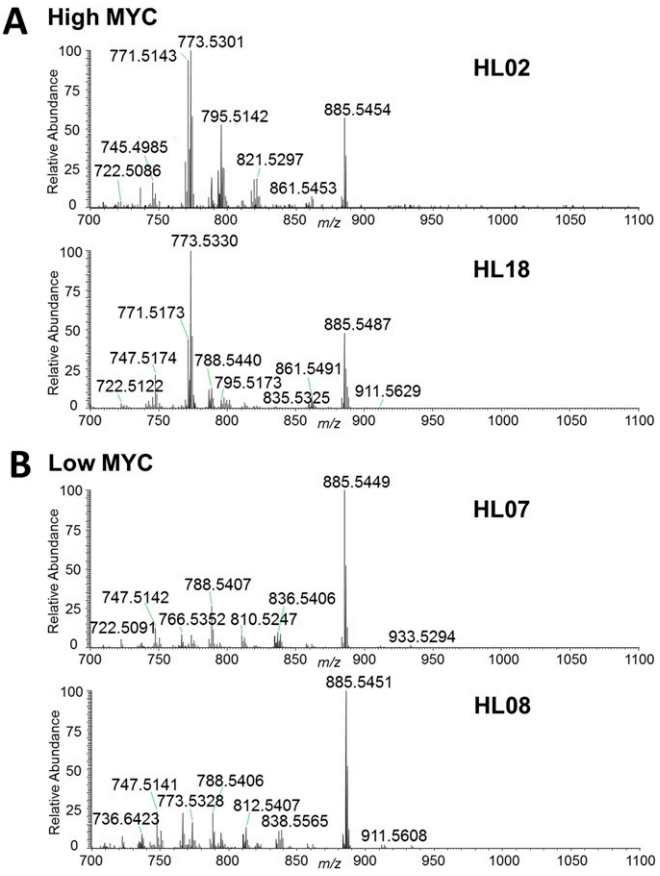

Fig. S4. Representative negative ion mode DESI mass spectra of sample HL02, human DLBCL lymphoma with high expression of MYC (0.90 relative luminescence units, RLU), sample HL18, human Burkitt's lymphoma with high expression of MYC (0.95 RLU), sample HL07, human follicular lymphoma with low expression of MYC (0.13 RLU), and sample HL08, human follicular lymphoma with low expression of MYC (0.17 RLU).

1. Michalek RD, et al. (2011) Cutting edge: Distinct glycolytic and lipid oxidative metabolic programs are essential for effector and regulatory CD4+ T cell subsets. *J Immunol* 186(6):3299–3303.
2. Yang K, et al. (2013) T cell exit from quiescence and differentiation into Th2 cells depend on Raptor-mTORC1-mediated metabolic reprogramming. *Immunity* 39(6):1043–1056.

Table S1. Lipid species selected by SAM in increased or decreased abundance in MYC-induced lymphomas in comparison with normal control thymus tissue (FDR < 5%)

Increased in lymphoma				Decreased in lymphoma			
*m/z**	Attribution†	*m/z**	Attribution†	*m/z**	Attribution†	*m/z**	Attribution†
	PG		CL		PE		PS
743.4852	PG(18:2/16:1)	724.9864	CL(20:4/18:2/18:1/16:0)	722.5112	PE(P-16:0/20:4)	734.5328	PS(O-18:0/15:0)
745.5006	PG(18:1/16:1)	725.4924	CL(20:3/18:1/18:1/16:1)	730.5745	PE(P-16:0/20:0)	744.5163	PS(O-16:0/18:2)
767.4850	PG(18:1/18:4)	727.0014	CL(18:2/18:1/18:1/18:1)	746.5127	PE(P-16:0/22:6)	760.5119	PS(16:0/18:1)
769.5004	PG(16:0/20:4)	739.0022	CL(20:4/18:1/18:1/18:1)	750.5430	PE(P-18:0/20:4)	766.5015	PS(P-18:0/18:4)
771.5161	PG(18:2/18:1)			762.5067	PE(16:0/22:6)	770.5329	PS(P-18:0/18:2)
773.5321	PG(18:1/18:1)		acyl-PG	764.5225	PE(20:4/18:1)	782.4961	PS(18:4/18:0)
775.5501	PG(18:0/18:1)	1,033.7451	acyl-PG(18:2/18:1/16:0)	766.5379	PE(18:0/20:4)	784.5120	PS(18:0/18:3)
793.5003	PG(18:2/20:4)	1,035.7617	acyl-PG(18:1/18:1/16:0)	776.5221	PE(22:4/17:2)	786.5275	PS(18:0/18:2)
795.5163	PG(20:4/18:1)	1,057.7447	acyl-PG(18:1/18:2/18:2)	778.5378	PE(20:4/19:1)	788.5435	PS(18:0/18:1)
797.5330	PG(20:4/18:0)	1059.7606	acyl-PG(18:1/18:1/18:2)	790.5382	PE(18:0/22:6)	792.5171	PS(P-18:0/20:5)
799.5498	PG(20:2/18:1)			792.5542	PE(20:1/20:4)	794.5329	PS(P-18:0/20:4)
817.5003	PG(20:4/20:4)		PE	794.5693	PE(18:0/22:4)	806.4963	PS(16:0/22:6)
819.5163	PG(18:1/22:6)	716.5220	PE(16:0/18:1)	802.5372	PE(19:1/22:6)	808.5125	PS(20:5/18:0)
821.5322	PG(18:2/22:4)	740.5220	PE(18:1/18:2)	804.5530	PE(22:6/19:0)	810.5275	PS(18:0/20:4)
823.5479	PG(22:4/18:1)	742.5375	PE(18:0/18:2)			812.5437	PS(18:0/20:3)
825.5687	PG(22:4/18:0)				PI	818.5325	PS(P-18:0/22:6)
827.5838	PG(18:1/22:2)		PI	833.5163	PI(16:0/18:2)	820.5486	PS(O-18:0/22:6)
841.5001	PG(20:4/22:6)	859.5333	PI(18:2/18:1)	857.5167	PI(20:4/16:0)	822.5649	PS(P-18:0/22:4)
843.5166	PG(20:3/22:6)	861.5475	PI(18:0/18:2)	883.5322	PI(18:1/20:4)	834.5275	PS(18:0/22:6)
845.5318	PG(20:2/22:6)	887.5679	PI(18:0/20:3)	885.5478	PI(18:0/20:4)	836.5440	PS(18:0/22:5)
				909.5476	PI(18:0/22:6)	838.5592	PS(18:0/22:4)
849.5636	PG(20:2/22:4)		PS	911.5640	PI(18:0/22:5)		
869.5319	PG(22:6/22:4)	758.4959	PS(18:2/16:0)	914.5817	PI(18:0/22:4)		PA
873.5630	PG(22:4/22:4)	814.5593	PS(20:2/18:0)	933.5330	PI(20:2/22:6)	723.4952	PA(20:4/18:0)
			PA		CL		PG
		771.6269	PA(O-20:0/22:1)	723.4768	CL(18:2/18:2/18:2/18:2)	747.5166	PG(16:0/18:1)

*Measured *m/z* value is given. Exact *m/z*, mass errors, chemical formulas, and statistical scores for each lipid identified are given in Tables S2 and S3.
†Tentative identification was performed using high mass resolution–high mass accuracy and tandem mass spectrometry analyses. PE, glycerophosphoethanolamine; CL, cardiolipin; PG, glycerophosphoglycerols; PS, glycerophosphoserines; PA, glycerophosphate; PI, glycerophosphoinositols; (X:Y) denotes the total number of carbons and double bonds in the FA acid chains.

Table S2. Lipid species selected by SAM as increased in lymphoma (FDR < 5%) identified using high mass resolution–high mass accuracy and tandem mass spectrometry analyses

Measured *m/z*	SAM score (d)	Lipid class*	Tentative attribution	Exact *m/z*	Mass error (ppm)†	Proposed formula
716.5220	0.259	PE	PE(16:0/18:1)	716.5236	−2.13	$C_{39}H_{76}NO_8P$
740.5220	1.379		PE(18:1/18:2)	740.5236	−1.81	$C_{41}H_{75}NO_8P$
742.5375	1.317		PE(18:0/18:2)	742.5392	−2.31	$C_{41}H_{77}NO_8P$
724.9864	0.114	CL	CL(20:4/18:2/18:1/16:0)	724.9883	−2.62	$C_{81}H_{142}O_{17}P_2$
725.4924	0.736		CL(20:3/18:1/18:1/16:1)	725.4945	−2.89	$C_{81}H_{144}O_{17}P_2$
727.0014	0.612		CL(18:2/18:1/18:1/18:1)	727.004	−3.58	$C_{81}H_{146}O_{17}P_2$
739.0022	0.550		CL(20:4/18:1/18:1/18:1)	739.004	−2.71	$C_{83}H_{146}0_{17}P_2$
743.4852	2.333	PG	PG(18:2/16:1)	743.4869	−2.18	$C_{40}H_{72}O_{10}P$
745.5006	2.333		PG(18:1/16:1)	745.5025	−2.56	$C_{40}H_{74}O_{10}P$
767.4850	2.333		PG(18:1/18:4)	767.4869	−2.49	$C_{42}H_{72}O_{10}P$
769.5004	2.333		PG(16:0/20:4)	769.5025	−2.70	$C_{42}H_{74}O_{10}P$
771.5161	2.333		PG(18:2/18:1)	771.5182	−2.62	$C_{42}H_{76}O_{10}P$
773.5321	2.333		PG(18:1/18:1)	773.5338	−2.27	$C_{42}H_{78}O_{10}P$
775.5501	2.022		PG(18:0/18:1)	775.5495	0.82	$C_{42}H_{80}O_{10}P$
793.5003	2.333		PG(18:2/20:4)	793.5025	−2.75	$C_{44}H_{74}O_{10}P$
795.5163	2.333		PG(20:4/18:1)	795.5182	−2.29	$C_{44}H_{76}O_{10}P$
797.5330	2.333		PG(20:4/18:0)	797.5338	−1.01	$C_{44}H_{78}O_{10}P$
799.5498	2.333		PG(20:2/18:1)	799.5495	0.43	$C_{44}H_{80}O_{10}P$
817.5003	2.333		PG(20:4/20:4)	817.5025	−2.73	$C_{46}H_{74}O_{10}P$
819.5163	2.333		PG(18:1/22:6)	819.5182	−2.24	$C_{46}H_{76}O_{10}P$
821.5322	2.333		PG(18:2/22:4)	821.5338	−1.99	$C_{46}H_{78}O_{10}P$
823.5479	2.333		PG(22:4/18:1)	823.5495	−1.94	$C_{46}H_{80}O_{10}P$
825.5687	2.001		PG(22:4/18:0)	825.5651	4.35	$C_{46}H_{82}O_{10}P$
827.5838	2.022		PG(18:1/22:2)	827.5808	3.72	$C_{46}H_{84}O_{10}P$
841.5001	1.587		PG(20:4/22:6)	841.5025	−2.83	$C_{48}H_{74}O_{10}P$
843.5166	1.255		PG(20:3/22:6)	843.5182	−1.91	$C_{48}H_{76}O_{10}P$
845.5318	2.229		PG(20:2/22:6)	845.5338	−2.35	$C_{48}H_{78}O_{10}P$
849.5636	2.146		PG(20:2/22:4)	849.5651	−1.78	$C_{48}H_{82}O_{10}P$
869.5319	0.238		PG(22:6/22:4)	869.5338	−2.15	$C_{50}H_{78}O_{10}P$
873.5630	1.400		PG(22:4/22:4)	873.5651	−2.45	$C_{50}H_{82}O_{10}P$
758.4959	0.529	PS	PS(18:2/16:0)	758.4978	−2.50	$C_{40}H_{73}NO_{10}P$
814.5593	0.798		PS(20:2/18:0)	814.5604	−1.27	$C_{44}H_{81}NO_{10}P$
771.6269	0.036	PA	PA(O-20:0/22:1)	771.6273	−0.59	$C_{45}H_{88}O_7P$
859.5333	0.747	PI	PI(18:2/18:1)	859.5342	−1.05	$C_{45}H_{80}O_{13}P$
861.5475	1.856		PI(18:0/18:2)	861.5499	−2.77	$C_{45}H_{82}O_{13}P$
887.5679	0.612		PI(18:0/20:3)	887.5655	2.72	$C_{47}H_{84}O_{13}P$
1033.7451	1.867	acyl-PG	acyl-PG(18:2/18:1/16:0)	1,033.7478	−2.61	$C_{60}H_{106}O_{11}P$
1035.7617	2.022		acyl-PG(18:1/18:1/16:0)	1,035.7635	−1.74	$C_{60}H_{108}O_{11}P$
1057.7447	1.275		acyl-PG(18:1/18:2/18:2)	1,057.7478	−2.93	$C_{62}H_{106}O_{11}P$
1059.7606	1.711		acyl-PG(18:1/18:1/18:2)	1,059.7635	−2.74	$C_{62}H_{108}O_{11}P$

*PE, glycerophosphoethanolamine; PS, glycerophosphoserines; PI, glycerophosphoinositols; CL, cardiolipin; PA, glycerophosphate; PG, glycerophosphoglycerols; (X:Y) denotes the total number of carbons and double bonds in the FA chains.

†Mass errors were calculated based on the exact monoisotopic *m/z* of the deprotonated form of the assigned molecules.

Table S3. Lipid species selected by SAM as decreased in lymphoma (FDR < 5%) identified using high mass resolution/high mass accuracy and tandem mass spectrometry analyses

Measured *m/z*	SAM score (d)	Lipid class*	Tentative attribution	Exact *m/z*	Mass error (ppm)†	Proposed formula
722.5112	−2.333	PE	PE(P-16:0/20:4)	722.5130	−2.1	$C_{41}H_{73}O_7NP$
730.5745	−0.778		PE(P-16:0/20:0)	730.5756	−1.5	$C_{41}H_{81}O_7NP$
746.5127	−2.333		PE(P-16:0/22:6)	746.5130	−0.6	$C_{43}H_{73}O_7NP$
750.5430	−1.918		PE(P-18:0/20:4)	750.5443	−1.7	$C_{43}H_{77}O_7NP$
762.5067	−1.981		PE(16:0/22:6)	762.5079	−1.7	$C_{43}H_{73}O_8NP$
764.5225	−1.711		PE(20:4/18:1)	764.5236	−1.4	$C_{43}H_{75}O_8NP$
766.5379	−2.333		PE(18:0/20:4)	766.5392	−1.8	$C_{43}H_{77}O_8NP$
776.5221	−1.400		PE(22:4/17:2)	776.5236	−1.8	$C_{44}H_{75}O_8NP$
778.5378	−1.587		PE(20:4/19:1)	778.5392	−1.8	$C_{44}H_{77}O_8NP$
790.5382	−1.587		PE(18:0/22:6)	790.5392	−1.3	$C_{45}H_{77}O_8NP$
792.5542	−1.244		PE(20:1/20:4)	792.5549	−0.8	$C_{45}H_{79}O_8NP$
794.5693	−1.628		PE(18:0/22:4)	794.5705	−1.5	$C_{45}H_{81}O_8NP$
802.5372	−1.244		PE(19:1/22:6)	802.5392	−2.6	$C_{46}H_{77}O_8NP$
804.5530	−1.006		PE(22:6/19:0)	804.5549	−2.3	$C_{46}H_{79}O_8NP$
734.5328	−0.798	PS	PS(O-18:0/15:0)	734.5342	−1.8	$C_{39}H_{77}O_9NP$
744.5163	−0.819		PS(O-16:0/18:2)	734.5185	−3.0	$C_{40}H_{75}O_9NP$
760.5119	−2.292		PS(16:0/18:1)	760.5134	−2.0	$C_{40}H_{75}O_{10}NP$
766.5015	−2.053		PS(P-18:0/18:4)	766.5029	−1.7	$C_{42}H_{73}O_9NP$
770.5329	−0.798		PS(P-18:0/18:2)	770.5342	−1.6	$C_{42}H_{77}O_9NP$
782.4961	−0.933		PS(18:4/18:0)	782.4978	−2.1	$C_{42}H_{73}O_{10}NP$
784.5120	−0.705		PS(18:0/18:3)	784.5134	−1.8	$C_{42}H_{75}O_{10}NP$
786.5275	−1.711		PS(18:0/18:2)	786.5291	−2.0	$C_{42}H_{77}O_{10}NP$
788.5435	−2.333		PS(18:0/18:1)	788.5447	−1.6	$C_{42}H_{79}O_{10}NP$
792.5171	−1.773		PS(P-18:0/20:5)	792.5185	−1.7	$C_{44}H_{75}O_9NP$
794.5329	−2.333		PS(P-18:0/20:4)	794.5342	−1.6	$C_{44}H_{77}O_9NP$
806.4963	−2.188		PS(16:0/22:6)	806.4978	−1.8	$C_{44}H_{73}O_{10}NP$
808.5125	−0.985		PS(20:5/18:0)	808.5134	−1.1	$C_{44}H_{75}O_{10}NP$
810.5275	−2.333		PS(18:0/20:4)	810.5291	−2.0	$C_{44}H_{77}O_{10}NP$
812.5437	−2.333		PS(18:0/20:3)	812.5447	−1.3	$C_{44}H_{79}O_{10}NP$
818.5325	−1.867		PS(P-18:0/22:6)	818.5342	−2.0	$C_{46}H_{77}O_9NP$
820.5486	−2.001		PS(O-18:0/22:6)	820.5498	−1.1	$C_{46}H_{79}O_9NP$
822.5649	−2.022		PS(P-18:0/22:4)	822.5655	−0.7	$C_{46}H_{81}O_9NP$
834.5275	−2.333		PS(18:0/22:6)	834.5291	−2.1	$C_{46}H_{77}O_{10}NP$
836.5440	−2.333		PS(18:0/22:5)	836.5447	−0.9	$C_{46}H_{79}O_{10}NP$
838.5592	−2.333		PS(18:0/22:4)	838.5604	−1.5	$C_{46}H_{81}O_{10}NP$
833.5163	−1.192	PI	PI(16:0/18:2)	833.5186	−2.7	$C_{43}H_{78}O_{13}P$
857.5167	−2.333		PI(20:4/16:0)	857.5186	−2.3	$C_{45}H_{78}O_{13}P$
883.5322	−1.607		PI(18:1/20:4)	883.5342	−2.4	$C_{47}H_{80}O_{13}P$
885.5478	−2.333		PI(18:0/20:4)	885.5499	2.2	$C_{47}H_{82}O_{13}P$
909.5476	−1.960		PI(18:0/22:6)	909.5499	−2.5	$C_{49}H_{82}O_{13}P$
911.5640	−1.234		PI(18:0/22:5)	911.5655	−1.6	$C_{49}H_{84}O_{13}P$
914.5817	−0.695		PI(18:0/22:4)	914.5845	−3.1	$C_{49}H_{86}O_{13}P$
933.5330	−2.333		PI(20:2/22:6)	933.5499	−18.1	$C_{51}H_{82}O_{13}P$
723.4768	−1.161	CL	CL(18:2/18:2/18:2/18:2)	723.4788	−2.8	$C_{81}H_{140}O_{17}P_2$
723.4952	−1.483	PA	PA(20:4/18:0)	723.4970	−2.5	$C_{41}H_{72}O_8P$
747.5166	−1.027	PG	PG(16:0/18:1)	747.5182	−2.1	$C_{40}H_{76}O_{10}P$

*PE, glycerophosphoethanolamine; PS, glycerophosphoserines; PI, glycerophosphoinositols; CL, cardiolipin; PA, glycerophosphate; PG, glycerophosphoglycerols; (X:Y) denotes the total number of carbons and double bonds in the fatty acid chains.
†Mass errors were calculated based on the exact monoisotopic *m/z* of the deprotonated form of the assigned molecules.